PNAS RESEARCH ARTICLE | IMMUNOLOGY AND INFLAMMATION OPEN ACCESS

Direct observation correlates NFκB cRel in B cells with activating and terminating their proliferative program

Haripriya Vaidehi Narayanan[a,b], Mark Y. Xiang[a,b], Yijia Chen[a,b], Helen Huang[a,b], Sukanya Roy[c], Himani Makkar[c], Alexander Hoffmann[a,b,1], and Koushik Roy[c,1]

Affiliations are included on p. 12.

Edited by Ellen Rothenberg, California Institute of Technology, Pasadena, CA; received July 19, 2023; accepted May 28, 2024

Antibody responses require the proliferative expansion of B cells controlled by affinity-dependent signals. Yet, proliferative bursts are heterogeneous, varying between 0 and 8 divisions in response to the same stimulus. NFκB cRel is activated in response to immune stimulation in B cells and is genetically required for proliferation. Here, we asked whether proliferative heterogeneity is controlled by natural variations in cRel abundance. We developed a fluorescent reporter mTFP1-cRel for the direct observation of cRel in live proliferating B cells. We found that cRel is heterogeneously distributed among naïve B cells, which are enriched for high expressors in a heavy-tailed distribution. We found that high cRel expressors show faster activation of the proliferative program, but do not sustain it well, with population expansion decaying earlier. With a mathematical model of the molecular network, we showed that cRel heterogeneity arises from balancing positive feedback by autoregulation and negative feedback by its inhibitor IκBε, confirmed by mouse knockouts. Using live-cell fluorescence microscopy, we showed that increased cRel primes B cells for early proliferation via higher basal expression of the cell cycle driver cMyc. However, peak cMyc induction amplitude is constrained by incoherent feedforward regulation, decoding the fold change of cRel activity to terminate the proliferative burst. This results in a complex nonlinear, nonmonotonic relationship between cRel expression and the extent of proliferation. These findings emphasize the importance of direct observational studies to complement gene knockout results and to learn about quantitative relationships between biological processes and their key regulators in the context of natural variations.

cRel fluorescent reporter | IκBε negative feedback | B cell proliferation | cell-to-cell heterogeneity | direct observation

Significance

B cells are capable of substantial stimulus-responsive proliferation, but also show substantial cell-to-cell proliferative heterogeneity. Gene-knockout models established that NFκB cRel is required for stimulus-driven B cell proliferation, but whether variability in its expression is responsible for proliferative heterogeneity remains unknown. In this study, we developed a fluorescent reporter mTFP1-cRel mouse to directly observe natural cRel variation in B cells and relate it to proliferation kinetics. We found that cRel abundance in naïve B-cells is highly heterogeneous due to combined positive and negative feedback. While high-cRel-expressing cells enter the proliferative program faster, they have diminished proliferative capacity. These findings resolve conflicting suggestions in the literature and emphasize the power of direct observation to understand how natural variation controls biological function.

Antibody responses arise from the selective proliferation of B cells in response to antigenic stimulus. Every B cell has a unique antigen receptor, and antigen recognition leads to pro-proliferative signals promoting B cell clonal expansion. This is characterized by a burst of multiple divisions following a single immunogenic stimulation. According to clonal selection theory, high-affinity B cells receive a strong stimulus and hence proliferate to a greater extent, while low-affinity B cells receive a weaker stimulus and so do not proliferate as much (1, 2). However, naïve B cells vary widely in their intrinsic capacity to proliferate, even under strongly pro-proliferative signals. Pioneering dye dilution experiments showed that during ex vivo stimulation in which all B cells are exposed to an identical affinity-independent stimulus, cells at any given timepoint are distributed across a range of different generations (3, 4). This indicates that there are nongenetic causes underlying heterogeneous B cell survival and proliferation decisions (5).

Much prior work using genetic knockout approaches has established that the nuclear factor kappa B (NFκB) family member Reticuloendotheliosis proto-oncogene (cRel) is essential for B cell population expansion (6–8). Single-cell live microscopy showed that one important role of cRel is to ensure cell survival, since *rel*$^{-/-}$ B cells entirely lacking in cRel remain susceptible to cell death after entering the growth phase, unlike their wild-type counterparts (9). However, while ectopic expression of anti-apoptotic factors rescues survival in *rel*$^{-/-}$ B cells, it does not restore their proliferative capacity, and population growth remains diminished (6). This suggests that cRel is also required for initiating B cell cycle entry. Overall, these gene knockout studies established that cRel is a key regulatory node in B cell proliferation, regulating cell survival and cell cycle entry. Studies of heterozygous *rel*$^{+/-}$ B cells also showed defects in a population-level DNA synthesis assay (7, 8). However, whether the cRel expression level in B cells is a driver of the phenotypic heterogeneity of single cells has not been addressed.

Quantitative relationships between naturally varying protein abundances and heterogeneity in function are best revealed by observing the natural variation for correlations.

Author contributions: H.V.N., A.H., and K.R. designed research; H.V.N., M.Y.X., Y.C., H.H., S.R., H.M., and K.R. performed research; H.V.N., M.Y.X., Y.C., H.H., S.R., H.M., and K.R. analyzed data; H.V.N., A.H., and K.R. wrote the paper; and all authors provided feedback.

The authors declare no competing interest.

This article is a PNAS Direct Submission.

[1]To whom correspondence may be addressed. Email: ahoffmann@ucla.edu or koushik.roy@path.utah.edu.

This article contains supporting information online at https://www.pnas.org/lookup/suppl/doi:10.1073/pnas.2309686121/-/DCSupplemental.

Published July 18, 2024.

This approach has been successful in model organisms for which many individuals are available (10–13). It is also leveraged in single-cell ribonucleic acid sequencing (RNA-seq) studies where messenger RNA (mRNA) abundances are used to define the non-genetic states of individual cells (14, 15), although they cannot associate these states with biological functionality. Therefore, identifying the molecular drivers of B cell proliferative heterogeneity requires direct observation of their abundances in founder B cells and further relating them to subsequent stimulus-dependent proliferation characteristics.

In the absence of a suitable experimental method, we previously leveraged the availability of a dynamical systems model of the B cell molecular network that controls survival and proliferation in response to stimulus (5). This computational model recapitulates the observed heterogeneity in founder B cell proliferative expansion. LASSO regression on molecular species represented in the model identified the abundances of apoptotic regulators Bim, Bcl2, and Bax as most correlated with proliferative expansion, more so than regulators in the signaling pathways or cell cycle control module (5). This computational modeling-based result was surprising, given the expectation of cRel's central role based on aforementioned gene knockout experimental studies.

Here, we directly examined the relationship between cRel expression in founder B cells and their subsequent stimulus-responsive proliferative expansion. We generated a fluorescent reporter mTFP1-cRel mouse strain to report on the abundance of cRel expression in individual B cells in a nondestructive manner. This enabled us to quantify the degree of heterogeneity of cRel abundance in live intact B cells, sort B cell populations based on cRel abundance, and measure differences in their proliferative outcomes by dye dilution. We unexpectedly found that cRel abundance and B cell proliferation are not proportional, but have a complex relationship in which some characteristics of proliferative clonal expansion are enhanced by cRel but others are diminished. We show that this may underlie the proliferation phenotypes of marginal zone vs. follicular B cell subsets. We identify the IκBε negative feedback loop as a regulatory mechanism for how such heterogeneity in cRel abundance—and hence proliferative expansion—is generated and maintained in B cells. Using live cell imaging, we further reveal a nonlinear relationship with the cRel target gene cMyc which drives the cell cycle, whose expression is constrained by an incoherent feedforward loop that decodes the fold change of cRel activity. Our results support the notion that proliferative heterogeneity driven by cRel abundance is an intrinsic feature of the B cell response to immune stimulation.

Results

A mTFP1-cRel Knock-In Reporter Mouse Strain. To measure the abundance of cRel in live naïve splenic B cells, we produced a knock-in mouse strain with a fluorescent fusion reporter mTFP1-cRel. The 5′ untranslated region (UTR) of the cRel gene is 271 nucleotides and confined to the first exon which overlaps with core promoter elements (and a CTCF binding site) that may mediate the regulation of cell type-specific or stimulus-induced transcription. Hence, we inserted the fluorescent protein monomeric teal fluorescent protein 1 (mTFP1) [along with a short flexible linker $(G4S)_2$] after amino acid position 6, which is near the start of the second exon. We duplicated amino acids 5 and 6 after the insertion, to preserve the functionally important Rel homology domain (RHD) which is between amino acid positions 8 to 297 (Fig. 1*A*). This design aimed to avoid disrupting the transcriptional regulatory regions controlling the cell-type-specific and stimulus-responsive expression of cRel. The germline mutation to yield the mTFP1-cRel mouse strain was produced through classical embryonic stem cell recombination and blastocyst complementation.

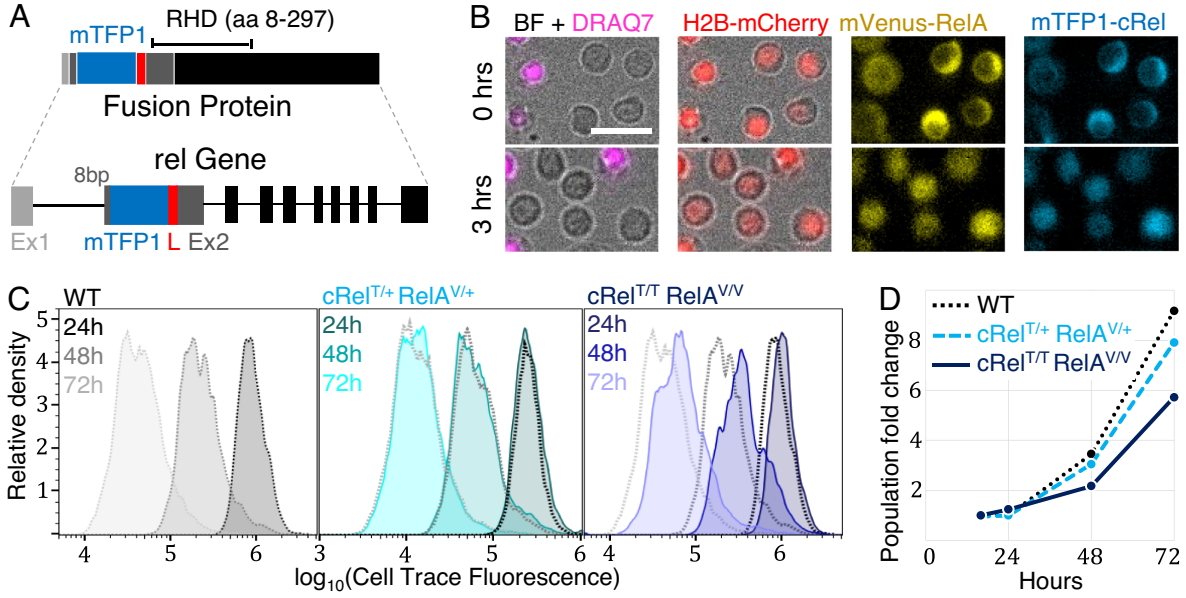

Fig. 1. The mTFP1-cRel reporter has similar expression & functional activity as WT cRel and complements a mVenus-RelA reporter for multimodal studies in live primary B-cells. (*A*) Schematic of the mTFP1-cRel fusion reporter construct. The mTFP1 fluorescent protein (mTFP1, blue) is inserted within Exon 2 of cRel (Ex2, dark gray) with a flexible linker (L, red), for better stability of the fusion product. The RHD is also indicated. (*B*) Multichannel fluorescence microscopy images of live heterozygous dual-reporter B-cells at 40X/NA1.3 under oil immersion. Panels in order show brightfield images with DRAQ7 viability staining (deep red), H2B-mCherry (red) as a marker distinguishing cytoplasmic and nuclear compartments, with mVenus-RelA (yellow) and mTFP1-cRel (blue) cellular localization compared at 0 h baseline and 3 h poststimulation with CpG. (*C*) Dye dilution assay with Cell Trace Far Red comparing generation numbers and proportions across all time-points, for wild-type B cells (*Left*), heterozygous $cRel^{mTFP1/+}$ $RelA^{mVenus/+}$ dual-reporter B cells (*Middle* panel solid curves), and homozygous $cRel^{mTFP1/mTFP1}$ $RelA^{mVenus/mVenus}$ dual-reporter B cells (*Right* panel solid curves). The corresponding wild-type dotted curves are superimposed on the *Middle* and *Right*. (*D*) Cell counts show kinetic trends of population expansion for wild-type B cells (dotted line), heterozygous dual-reporter B cells (dashed line), and homozygous dual-reporter B cells (solid line).

To test the design of the reporter, we first tested whether the fusion protein was expressed intact and without proteolysis, and at levels comparable to wild-type cRel, by immunoblotting whole cell lysates. We stimulated heterozygous cRel$^{mTFP1/+}$ B cells for 24, 48, and 72 h with different ligands—LPS, CpG, and anti-IgM—to confirm that the two alleles had comparable expression dynamics over time under all stimulations (*SI Appendix*, Fig. S1*A*). By comparing these against lysates from wild-type B cells, we verified that the presence of the reporter allele did not itself skew cRel expression over time.

Stimulation of B cells with immunogenic ligands activates nuclear cRel:p50 to carry out functions as a transcription factor. Electrophoretic mobility shift assays (EMSAs) on the nuclear fraction with a radioactive oligonucleotide probe containing a κB binding site showed that mTFP1-cRel which translocates to the nucleus is equally capable of binding DNA as wild-type cRel. Further antibody supershifts confirmed the identity and composition of the complexes (*SI Appendix*, Fig. S1*B*). Together, our results confirmed that the mTFP1-cRel reporter performs signaling and DNA binding functions with efficiencies comparable to its wild-type counterpart. This complements another fluorescent fusion protein cRel reporter that was recently made available, whose utility for a number of applications has also been documented (16).

In addition to cRel, the NFκB family member RelA has also been shown to play a role in determining B cell responses to stimulation (8, 17, 18). In previous work, we had generated a mVenus-RelA reporter mouse strain, to enable high-throughput live cell studies of macrophages (19). Here, we cross-bred both strains to produce dual-reporter mice that enable simultaneous measurement of both NFκB cRel and RelA in B cells. By immunoblotting both cytoplasmic (*SI Appendix*, Fig. S1*C*) and nuclear (*SI Appendix*, Fig. S1*D*) lysates, we showed that both reporter proteins have similar expression and signaling dynamics as their wild-type counterparts, over long time-courses of 120 h. EMSAs on the nuclear fraction from heterozygous dual-reporter B cells allowed us to quantify DNA binding activity, showing that the reporter and wild-type alleles have evenly matched DNA binding capabilities (*SI Appendix*, Fig. S1*E*). Thus, we confirmed that both reporters can be functionally combined in B cells with minimal regulatory interference.

In addition to flow cytometry, this combination of reporters is also suitable for visualization by live-cell multichannel fluorescence microscopy. Naïve B cells are approximately 5 μm in size, with most of the cell volume occupied by a large nucleus around 3 to 4 μm in diameter. To address the challenge of resolving the nuclear compartment and the thin cytoplasm (<1 μm), we developed a workflow to image B cells at high magnification under oil immersion. We cross-bred mTFP1-cRel mVenus-RelA dual reporter mice with a H2B-mCherry strain (Jackson laboratories) to mark the nucleus, and employed a viability stain (DRAQ7 or AnnexinV-CF647) in the far-red wavelength spectrum (Fig. 1*B* and *SI Appendix* SV1 and SV2). These spectra can be easily visualized using the commonly available CFP/YFP/mCherry/Cy5 combination of imaging filters (*SI Appendix*, Fig. S1*F*). Using single reporter B cells, we confirmed the absence of cross-bleed between mTFP1-cRel and mVenus-RelA signals (*SI Appendix*, Fig. S1*G*), allowing independent measurement of each without additional spectral compensation. Together, this allowed us to distinguish cytoplasmic cRel and RelA, bound by the IκB proteins which inhibit their signaling activity, from their active fractions that translocate to the nucleus upon stimulation (Fig. 1*B* and *SI Appendix* SV3).

We then investigated whether the activity of mTFP1-cRel or mVenus-RelA alters the functional outcome of proliferative expansion in response to NFκB signaling in stimulated B cells. Flow cytometry-based dye dilution assays with Cell Trace Far Red showed almost identical proportions of wild-type and heterozygous dual-reporter cRel$^{mTFP1/+}$ RelA$^{mVenus/+}$ B cells reaching the same generations at the same time, while homozygous cRel$^{mTFP1/mTFP1}$ RelA$^{mVenus/mVenus}$ B cells had slightly reduced proliferation capacity in reaching the terminal generation (Fig. 1*C*). The net fold increase of the population after stimulation was slightly lower in dual-reporter B cells compared to wild-type counterparts (Fig. 1*D*). Heterozygous dual-reporter B cells showed a 6% reduction in total cell number at 72 h, and homozygous reporter B cells showed a 27% decline. We conclude that the homozygous reporter may be preferable to track cRel or RelA expression in live cells, while heterozygosity may be preferable for functional assays.

In sum, we established that our mTFP1-cRel fusion reporter is equivalent to wild-type cRel in its signaling and DNA binding activities, compatible with our existing mVenus-RelA reporter, and allows functional studies relating NFκB abundance to B cell proliferative expansion in heterozygous reporter B cells by flow cytometry and live cell microscopy.

Heterogeneous cRel Expression among Splenic B Cells. Our first step was to evaluate how the steady-state abundance of cRel is distributed across a population of naïve splenic reporter B cells using flow cytometry (Fig. 2*A*). We chose to use homozygous cRel$^{mTFP1/mTFP1}$ B cells to ensure that we capture the entire abundance of intracellular cRel. We found that the distribution of cRel across B cell populations is heterogenous, with a coefficient of variation (CV) around 0.38, i.e., the SD on either side is 38% of the mean, with about a fourfold difference in cRel expression between the top and bottom 1% of cells. The statistical moments of this distribution were found to be highly consistent across four mice of different ages, sexes, litters, and even vivaria (CV = 0.38 ± 0.04, skew = 2 ± 0.4, kurtosis = 7.5 ± 3.2) (Fig. 2*B*). While earlier studies measured a typical range of CVs between 0.15 and 0.3 in mammalian cells (20), higher levels of variation in signaling proteins (CV > 0.5) were shown to mediate functional differences in the response of T-cells to antigens (21), suggesting that variation in cRel expression may also influence B cell stimulus responses.

Expression distributions of a cellular protein or transcription factor are approximated as log-normal (20, 22, 23). This was observed in our B cell populations for the cell-type-specific surface marker B220. However, fitting a lognormal curve to our data revealed that the distribution of cRel had heavier tails than expected—particularly the right tail corresponding to cells with increased cRel abundance (Fig. 2*A*). This was confirmed by consistently positive measures of skew (2.0 ± 0.4), indicating a rightward imbalance toward increased cRel fluorescence. On a semilog-scale, the distribution is leptokurtic (with excess kurtosis of 7.5 ± 3.2 beyond the normal distribution), indicating greater presence of outliers. Since single statistical tests—particularly the Kolmogorov–Smirnov test—are considered unreliable for flow cytometry data, we performed a variety of other tests for log-normality. We found that the Shapiro–Wilk, Pearson–D'Agostino, and Anderson–Darling tests consistently rejected log-normality of cRel abundance, establishing the statistical significance of the heavy tails. By computing the density difference between the observed cRel distribution and its lognormal fit, we estimated that 4.2% of the cRel distribution density lies in the right tail. This indicates that the distribution of cRel is fat-tailed, and tends to be weighted toward high cRel-expressing B cells.

For a better description of the mathematical relationship between cRel abundance levels and their occurrence in the B cell population, we fit this distribution on a log–log scale (Fig. 2*C*), using the built-in optimization algorithm in the SciPy.stats package to scan parameters and minimize deviations between fit and

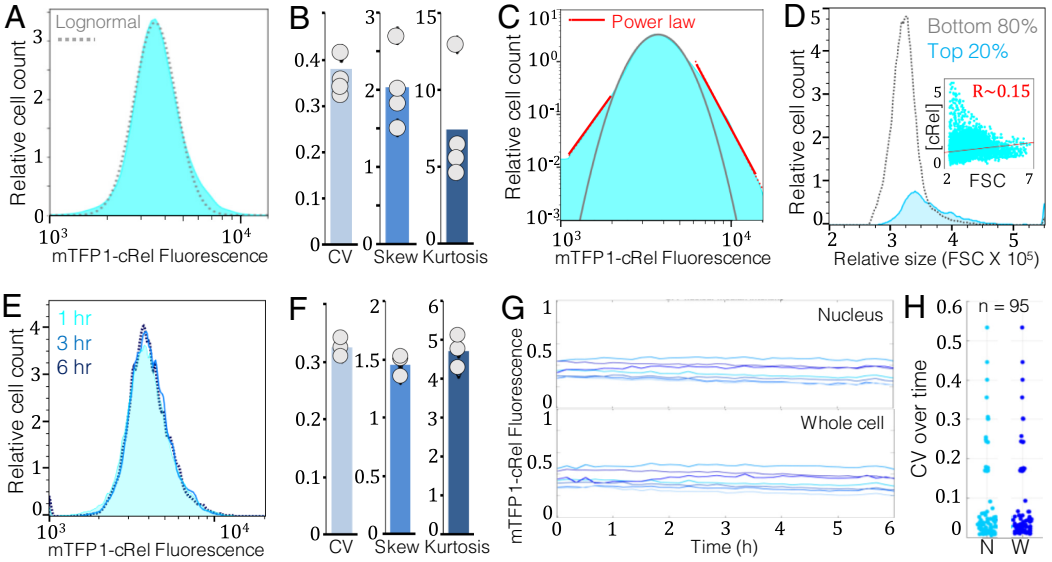

Fig. 2. The steady-state cellular abundance of cRel is heterogeneous with a heavy tail enriched for high expressors, reproducible across individuals, and stable over time. (*A*) Fluorescence distribution of mTFP1-cRel abundance in cRel$^{mTFP1/mTFP1}$ B cells, with a heavy-tail of high-expressing cells beyond expected log-normal frequencies. The dotted line shows the best-fit log-normal curve. (*B*) Statistical moments (CV, skew, kurtosis) for the shapes of cRel distributions across mice (n = 4). Each circle indicates one mouse. (*C*) mTFP1-cRel abundance approximates a log-normal distribution around the median, while the frequency of low- and high-expressing cells in the heavy tails can be fit to power-law distributions. (*D*) Distribution of cell size (as measured by forward scatter) for cells in the Top 20% of cRel expression (solid shaded curve), compared to the remaining 80% (dotted curve). (*D—Inset*) Scatter plot of relative cell size (linear scale, measured proportional to FSC) and relative cRel concentration (linear scale, measured as fluorescence/FSC), showing approximate regression line in red. (*E*) Stability analysis of population-level mTFP1-cRel fluorescence distribution in freshly isolated naïve B cells, for 6 h in the absence of immune stimulation. (*F*) Statistical moments (CV, skew, kurtosis) for cRel distribution shape across time (1 h, 3 h, and 6 h) in the same mouse. Each circle indicates one time point. (*G*) Representative trajectories of mTFP1-cRel fluorescence intensity for single naïve B-cells over 6 h in the absence of stimulation, measured by live cell microscopy. The *Top* plot shows median intensity in the nuclear compartment, while the *Bottom* plot shows mean intensity for the whole cell. (*H*) Stability analysis at the single-cell level for mTFP1-cRel (n = 95 individual cells). Each dot represents the CV across the trajectory of a single cell over 6 h. Distributions are shown for median nuclear intensity (N) and mean intensity of the whole cell (W).

data. We found that a log-normal distribution was able to adequately fit the central portion of the distribution. However, the heavy tails were better fit to power-law relationships (using manual adjustments to automated fits). This indicates that the shape of the cRel abundance distribution shape can be better described as Pareto log-normal (PLN), which is characterized by heavy tails around a central log-normal portion, suggesting a potential effect of feedback loops superimposed on random processes in generating this distribution (24).

We considered the possibility that the heterogeneity in cRel abundance may simply be an effect of larger cells having greater protein abundances. To investigate the relationship between cRel abundance and cell size, we divided the population into the top 20% and the bottom 80% of cRel expressors and superimposed their cell size distributions as measured by forward scatter (FSC). Rather than segregating by cRel abundance, we found that both the highest cRel expressors and the remaining population had overlapping cell size distributions (Fig. 2*D*). Further, the variability in cell size (CV = 0.15 ± 0.02) was much lower than the variation in cRel abundance (CV = 0.38 ± 0.04), indicating that size variations cannot fully explain the distribution of cRel abundance. We analyzed this relationship further by looking at the concentration of cRel within cells, measured as fluorescence/FSC, which may be more functionally relevant to signaling responses. Using a linear regression analysis, we found a low correlation between cRel concentration and cell size, with Pearson coefficient R = 0.18 ± 0.06 across four animals (Fig. 2 *D*, *Inset*). We corroborated these flow observations using single-cell microscopy for 95 individual cells, where the median intensity had a similarly low correlation of R = 0.19 with the cell area, confirming that cRel abundance and concentration are relatively independent of cell size.

In order to gauge how closely the measured ex vivo distributions may approximate the true in vivo distribution of cRel abundance, we determined its stability by sampling the same population periodically over 6 h in the absence of stimulation. Measurements of mTFP1-cRel fluorescence over this period show that the distribution remains steady, confirmed by a Jensen–Shannon divergence metric (JSD) of approximately 0 between the 1-, 3-, and 6-h time points (where a JSD of 0 indicates statistically identical distributions with complete overlap, while a JSD of 1 indicates complete separation) (Fig. 2*E*). Further, the statistical moments remained highly consistent over time (CV = 0.33 ± 0.01, skew = 1.46 ± 0.06, kurtosis = 4.71 ± 0.34), confirming the stability of the shape (Fig. 2*F*).

We further investigated the stability of expression at the single-cell level using live-cell microscopy. Trajectories of both whole cell and nuclear fluorescence remained stable over an imaging duration of 6 h (Fig. 2*G*), with most cells displaying only small fluctuations within a CV less than 0.1 over this period (Fig. 2*H*). This implies that measured cRel abundances may closely reflect the true distribution of cRel expression within splenic naïve B cell populations in vivo, whose whole-cell levels and subcellular localization are both stably maintained. Thus, our results point toward cell-intrinsic, size-independent regulatory mechanisms that control and distribute steady-state cRel expression in B cells.

RelA Abundance Is Correlated with cRel but Cannot Compensate for cRel Loss. Having evaluated cRel expression in naïve splenic B cells, we further looked at RelA abundance and its influence on proliferative outcomes in B cells. Similar to cRel, the expression of RelA is also heterogeneous and nonlognormal, with a heavy tail enriched for high expressors (*SI Appendix*, Fig. S2*A*). The statistical moments (CV = 0.24, skew = 2.8, excess kurtosis = 14.5) indicate that RelA has a narrower but more heavy-tailed distribution compared to cRel. Using live cell microscopy, we found that the expression levels and subcellular localization of RelA in single cells are also stable over time (*SI Appendix*, Fig. S2 *B* and *C*). We further measured cRel and RelA independently in dual-reporter B cells and showed that their expression and localization are strongly correlated, both under steady-state conditions (*SI Appendix*, Fig. S2 *E–G*) and poststimulation (*SI Appendix*, Fig. S2*H*).

RelA in the cytoplasm is typically bound by its signaling inhibitor IκBα. The steady-state distribution of RelA in the absence of IκBα remains unaffected compared to the wild type (*SI Appendix*, Fig. S2*D*), indicating that other IκB isoforms are sufficient to bind

available RelA and prevent RelA upregulation. Prior knockout studies have indicated that RelA may be able to sustain stimulus-responsive cell growth in $cRel^{-/-}$ B cells (7). We asked whether this is enhanced by elevated RelA. Using dye dilution assays, we found no effect of elevated RelA on proliferative capacity, as $I\kappa B\alpha^{\kappa B/\kappa B}$ B cells [where the negative feedback inhibition of RelA is disrupted, resulting in elevated induced RelA levels (25)] were comparable to the wild type. Likewise, we found that $cRel^{-/-}I\kappa B\alpha^{-/-}$ (entirely lacking in IκBα) were similar to $cRel^{-/-}$ B cells (*SI Appendix*, Fig. S2*I*). Looking at population size and growth rate, we found that $I\kappa B\alpha^{\kappa B/\kappa B}$ may have a slight advantage over wild-type B cells, indicating that RelA may increase population expansion in the presence of cRel (*SI Appendix*, Fig. S2 *J* and *K*). However, this effect disappears when comparing $cRel^{-/-}I\kappa B\alpha^{-/-}$ and $cRel^{-/-}$ B cells, where increased RelA is unable to rescue the proliferation defects caused by the loss of cRel. We concluded that cRel is more important than RelA in driving stimulus-responsive B cell proliferative expansion, and hence focused on cRel abundance in the remainder of this manuscript.

The Abundance of cRel in Naïve B Cells Predicts Their Proliferation Dynamics. Given the high heterogeneity of cRel expression in naïve splenic B cells, we investigated whether cRel abundance influences the proliferative outcomes of B cells. Since diminished cRel results in proliferative defects (6–9), the naïve extrapolation is that cRel abundance in B cells should have a simple positive correlation with both their proliferative capacity and the total extent of proliferative expansion.

To test this simple relationship, we flow-sorted bulk naïve splenic B cells from the lowest and highest quartiles of cRel abundance, stained them with the passive Cell Trace Far Red dye, and cultured both populations under identical stimulus conditions to observe their proliferation kinetics via dye dilution (Fig. 3*A*). We confirmed the divergence of these two populations in cRel abundance with a postsorting purity check, comparing the sorted populations against the parent population (Fig. 3*B*). As expected, the $cRel^{low}$ population excluded high cRel-expressing B cells, while the $cRel^{high}$ population lacked low and moderate cRel-expressing cells. A computed Jensen–Shannon divergence metric (JSD) of 0.56 further confirmed a significant separation between the two distributions, with similar divergences consistently reproduced across six replicate experiments over four different days. We compared both cRel expression and proliferation kinetics in culture over a period of 72 h, using the 15-h time point as our baseline reference, to avoid artifacts from early cell death due to mechanical damage during isolation from the spleen.

We first measured the dynamics of cRel abundance following stimulation with CpG. cRel expression is driven by κB-elements in its promoter (26, 27). Consistent with this autoinduction, we found that all B cells further increased their cRel abundance in the first 48 h. Surprisingly, at 48 h, the $cRel^{low}$ B cells showed a higher cRel abundance than the $cRel^{high}$ population (*SI Appendix*, Fig. S3*A*). We plotted the fold changes in geometric mean fluorescence intensity (GMFI) for both populations, using GMFI of the $cRel^{low}$ B cells at 15 h as the common denominator for comparison (*SI Appendix*, Fig. S3*B*). Though GMFI of both populations peaked at 48 h, the rate of cRel fluorescence increase slowed down in $cRel^{high}$ B cells after 24 h, while $cRel^{low}$ B cells sustained a steep increase in cRel abundance up to 48 h. Both $cRel^{low}$ and $cRel^{high}$ populations reached the same diminished expression levels at 72 h, suggesting that stimulus-induced negative feedback could keep cRel expression in check over this longer period.

We compared the proliferative expansion kinetics in the two populations during the same period by dye dilution. The same pattern was observed across three replicate experiments at different doses of CpG. A representative dye dilution plot indicates that both populations reach the same maximum number of divisions by 72 h, with the first divisions occurring between 24 and 48 h (Fig. 3*C*). Most $cRel^{high}$ B cells had undergone 3 to 4 divisions by 48 h, with the greatest increase in generation number coming between 24 and 48 h. In contrast, this expansion was delayed in $cRel^{low}$ B cells, reaching only 2 divisions by 48 h, with the majority of divisions occurring between 48 and 72 h. Thus, we conclude that the abundance of cRel in naïve founder B cells determines the activation speed of entering the stimulus-induced proliferation program.

Quantifying the cell numbers reached during the proliferative program yielded a surprising finding. A representative plot of fold change increase in population size over time is shown, relative to the baseline of 15-h population size in undivided $cRel^{low}$ B cells from the same mouse (Fig. 3*D*). This baseline is similar in both populations, since early death due to mechanical damage is independent of cRel. In accordance with faster proliferative activation, the $cRel^{high}$ B cells reached their peak population size at 48 h, earlier than $cRel^{low}$ B cells which required 72 h to reach their peak. However, in all cases, the peak population fold change of $cRel^{high}$ B cells was always smaller than the corresponding peak for $cRel^{low}$ B cells. To allow the comparison of expansion across experiments with varying stimulus doses, we plotted the population growth rate, defined as the fold change at each time point relative to the previous one. While $cRel^{high}$ B cells had a higher growth rate up to 48 h, this dropped sharply at 72 h, unlike $cRel^{low}$ B cells which sustained their growth across this entire period (Fig. 3*E*). Proliferation analysis in FlowJo showed that the $cRel^{high}$ B cells underwent fewer divisions on average by 72 h, with lower proliferation and replication indices in all conditions. This means that increased cRel abundance in the founders may unexpectedly abrogate population growth.

In summary, we conclude that increased cRel accelerates B cell entry into the proliferative program, but also terminates population expansion earlier, resulting in a complex nonlinear relationship to proliferative dynamics.

Increased Steady-State cRel Expression in Marginal Zone B Cells. The above observations were made with total splenic B cells, which comprise a mixture of phenotypically and functionally divergent marginal zone and follicular B cells. Marginal zone B cells are considered "innate-like," with a rapid but limited proliferative response to innate immune ligands like CpG and LPS (28, 29), while follicular B cells are capable of entering a sustained program of T cell-dependent selection and expansion. Proliferative responses in B cells are also stimulus-dependent, with CpG inducing rapid proliferation followed by exhaustion, compared to delayed kinetics in LPS or anti-IgM stimulation.

To ensure that we capture intrinsic features of cRel-driven proliferation, independent of B cell subtype or stimulus, we repeated the sorting and dye dilution assay, using pure follicular B cells stimulated with LPS. We similarly observed earlier proliferation in $cRel^{high}$ follicular B cells, between 48 and 72 h, and delayed expansion in $cRel^{low}$ follicular B cells between 72 and 96 h (Fig. 3*F*). Correspondingly, population growth rates in $cRel^{high}$ follicular B cells slowed down first after 72 h, while $cRel^{low}$ follicular B cells sustained their expansion longer for up to 96 h (Fig. 3 *G* and *H*). Thus, we establish that cRel drives a pattern of accelerated but less sustained proliferation in B cells, regardless of the cell subtype, stimulus, or dose.

We then asked whether this could explain the known differences in proliferative phenotype between marginal zone and follicular B cells. Using flow cytometry, we distinguished the two subtypes within splenic B-cells using the markers CD21 and CD23 and

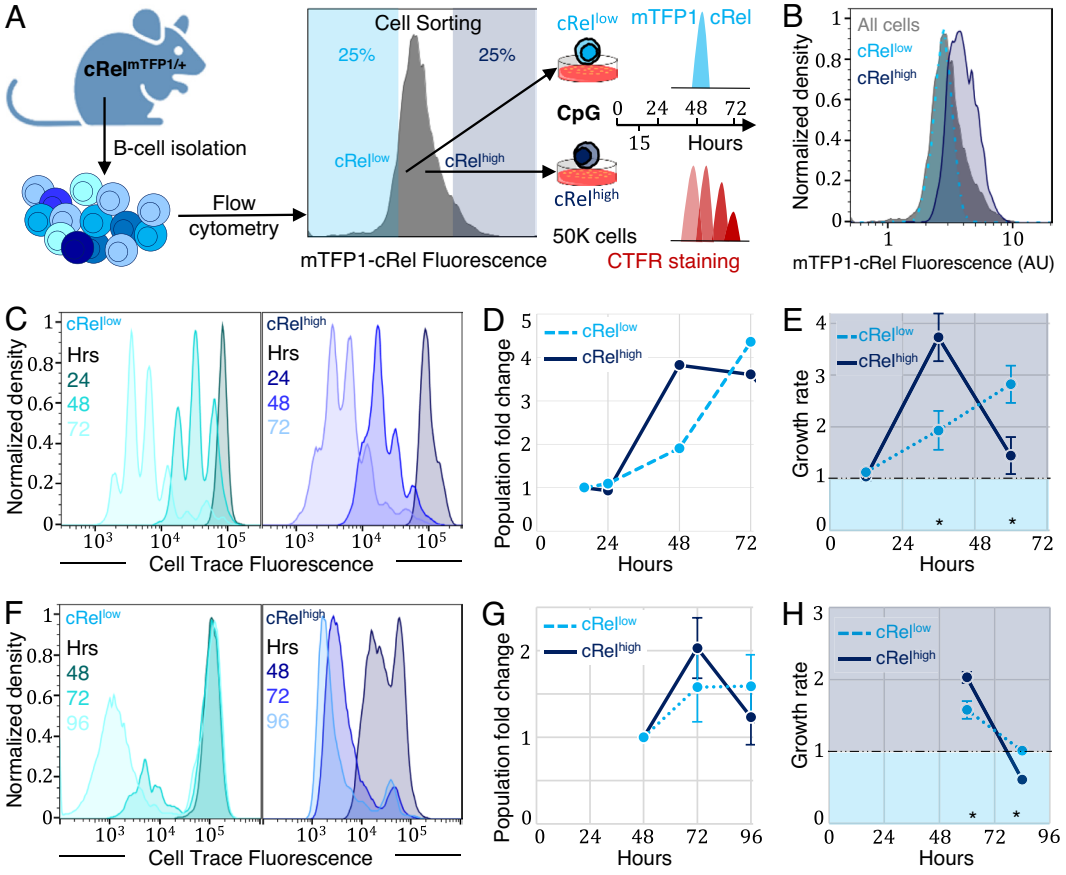

Fig. 3. Increased cRel abundance predicts both faster activation and termination of B cell proliferative dynamics upon stimulation. (*A*) Schematic of the experimental design to flow-sort B cells based on low (Bottom quartile) or high (Top quartile) mTFP1-cRel fluorescence intensity, and set up parallel dye dilution assays under identical stimulus conditions. (*B*) Mode-normalized fluorescence intensity distributions for postsorting purity check, showing cRel^{low} (light dotted curve) and cRel^{high} (dark solid curve), superimposed on the parent population (shaded curve), to compare enrichment of cells and divergence of the two populations (JSD = 0.56, where 0 = complete overlap and 1 = no overlap). (*C*) Representative mode-normalized fluorescence plots from dye dilution assays comparing proliferative capacities of cRel^{high} and cRel^{low} B cells, for total naïve splenic B-cells stimulated with CpG. (*D* and *E*) Representative line graphs of (*D*) population size over time (normalized to 14 h) and (*E*) growth rate (fold change per day), comparing cRel^{high} B cells (solid line) against cRel^{low} B cells (dotted line), for total naïve splenic B-cells stimulated with CpG. Observed trends for population size remain identical across three biological replicate experiments with varying doses of stimulus. Growth rate error bars are calculated for all three replicates pooled. The * marks time points at which differences are statistically significant with $P < 0.05$, using a *t* test. (*F*) Representative mode-normalized fluorescence plots from dye dilution assays comparing proliferative capacities of cRel^{high} and cRel^{low} B cells, for pure follicular naïve B-cells stimulated with LPS. (*G* and *H*) Line graphs of (*G*) population size over time (normalized to 48 h) and (*H*) growth rate (fold change per day), comparing cRel^{high} B cells (solid line) against cRel^{low} B cells (dotted line), for pure follicular naïve B-cells stimulated with LPS. Error bars cover biological replicates (n = 3), and the * marks time points at which differences are statistically significant with $P < 0.05$, using a *t* test.

measured the distribution of mTFP1-cRel in each. By comparing GMFIs, we found that marginal zone B cells reproducibly express about 60% higher cRel compared to follicular B cells from the same animal (*SI Appendix*, Fig. S4 *A* and *B*). Thus, increased expression of cRel at steady state may explain the rapid proliferation of marginal zone B cells in response to innate immune ligands.

The Noisy Negative Feedback Regulator IκBε Controls the Distribution of cRel Abundances and Kinetics of B Cell Proliferation. To explain the heterogeneity of cRel abundance in naïve splenic B cells, we considered the underlying regulatory mechanisms (Fig. 4*A*). The stable heavy-tailed distribution indicates cell-intrinsic feedback mechanisms controlling steady-state cRel. The positive feedback due to autoinduction of cRel expression (26, 27) may exacerbate small differences in expression, increasing the number of high-expressing cells. However, the nuclear activity of cRel is controlled by IκBε, which in turn is induced by nuclear cRel. This sets up a negative feedback loop (30) which may dampen expression. We hypothesized that the balance between positive and negative feedback determines cRel abundance, dynamics, and subsequent effects on B cell proliferation. Since the regulation of IκBε is known to be noisy and stochastic (30), we considered that the variable strength of the IκBε negative feedback loop among individual founder B cells is a determinant of their heavy-tailed distribution of cRel abundance.

To test whether IκBε affects the cRel abundance distribution in naïve B-cells, we first used a mathematical model which allows us to computationally alter the relative strengths of positive and negative feedback (5, 27). Since the variation in the strength of IκBε negative feedback is higher, we expect this to have a greater impact on cRel expression. When setting the negative feedback strength to zero, our simulation results predicted that the range of cRel abundance is similar, but the cRel distribution shapes in the wild type and IκBε$^{-/-}$ are different. The mean cRel abundance was predicted to be slightly higher (~5% more) in an IκBε$^{-/-}$ knockout compared to the wild type (Fig. 4*B*). More importantly, the predicted wild-type distribution had greater density in the lower half of the range, while the distribution in IκBε$^{-/-}$ B-cells was weighted more in the upper half of the range. Thus, we predicted that lack of IκBε negative feedback skews the distribution toward an increased number of high cRel expressing B cells.

To experimentally test this prediction, we crossed mTFP1-cRel reporter mice with IκBε$^{-/-}$ mice, and compared cRel abundance and B cell proliferation in the presence and absence of negative feedback regulation by IκBε. First, we measured cRel abundance in naïve cRel$^{mTFP1/mTFP1}$ IκBε$^{-/-}$ B cells. For better visualization, we normalized the distributions to allow direct comparison of probability densities, i.e., the relative frequencies of occurrence in the B cell population, across cRel abundance levels (Fig. 4*C*). Our measurements confirmed the computational predictions of a similar range of cRel abundance, but a higher mean and greater density at increased abundances for IκBε$^{-/-}$ B cells. We highlighted this change in distribution shape with abundance levels by plotting the difference in densities between IκBε$^{-/-}$ and wild-type B cells across the range of cRel abundance (Fig. 4*D*). Quantifying these differences showed that

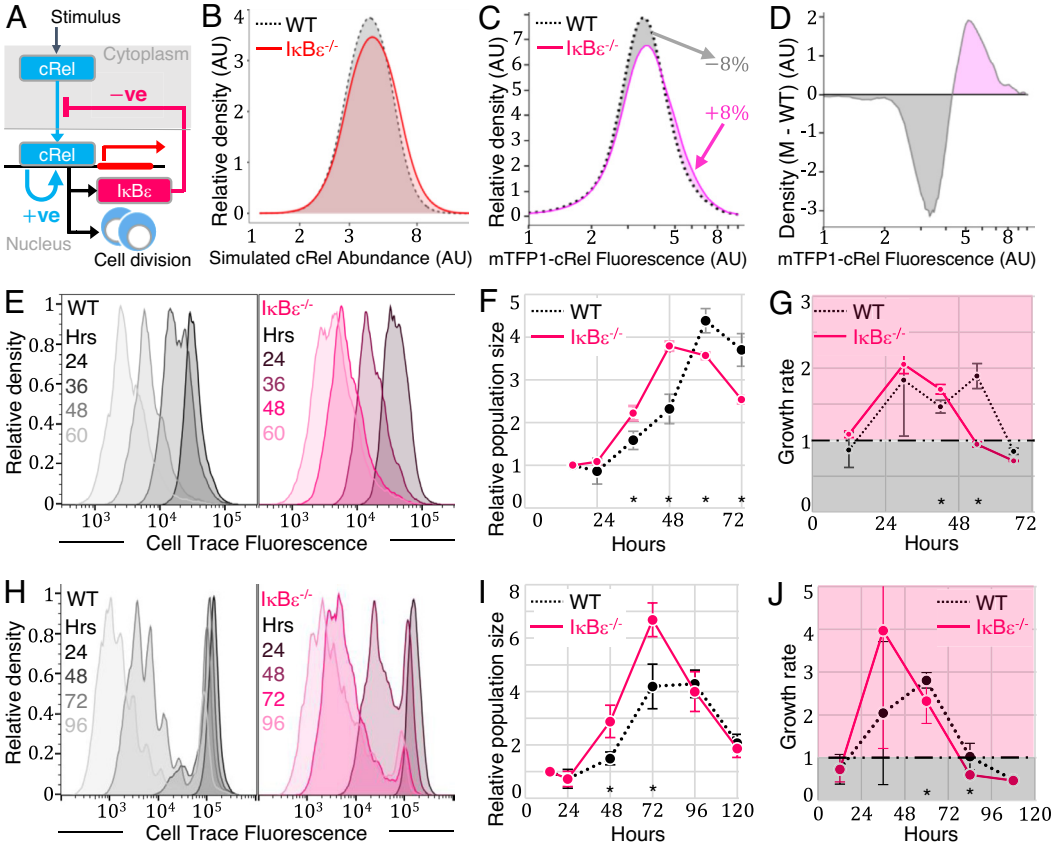

Fig. 4. Noisy negative feedback by IκBε distributes cRel among the B cell population, and controls the timing of proliferative activation and termination. (*A*) Schematic of negative feedback regulation of cRel dynamics and B cell proliferation, showing stimulus-induced cRel nuclear translocation, positive feedback loop due to autoinduction, and negative feedback loop due to inhibition of signaling by IκBε. (*B*) Simulation predicting the distribution of steady-state cRel abundance in B-cells in the absence of IκBε feedback (solid line, feedback strength set to zero for IκBε$^{-/-}$ in the model), compared to the wild type (WT, dotted line). (*C*) Distributions of cRel fluorescence in the wild type (cRel$^{mTFP1/mTFP1}$, dotted line) and negative feedback mutant cRel$^{mTFP1/mTFP1}$ IκBε$^{-/-}$ (solid line) total B cells. The black shaded region indicates where WT has greater density in the fluorescence distribution, whereas the pink shaded region shows where IκBε$^{-/-}$ B cells are enriched. Shape differences between distributions are upheld by a K-S test (*P*-value < 0.001) on the kernel density estimates, a binned Pearson chi-square test on the raw data (T ~ 75, given a baseline T_{min} ~ 4 for WT with respect to itself), as well as a Jensen–Shannon divergence metric of 0.08. (*D*) Difference in kernel density estimates of cRel fluorescence between wild-type (cRel$^{mTFP1/mTFP1}$) and cRel$^{mTFP1/mTFP1}$ IκBε$^{-/-}$ B cells highlight negative difference (i.e., WT has greater density) at moderate expression levels, and positive difference (i.e., IκBε$^{-/-}$ has greater density) at higher expression levels. (*E*) Representative mode-normalized fluorescence plots from dye dilution assays comparing the proliferative capacities of IκBε$^{-/-}$ and WT B cells, for total naïve splenic B-cells stimulated with CpG. (*F* and *G*) Representative line graphs of (*F*) population size over time (normalized to 14 h) and (*G*) growth rate (fold change per day), comparing IκBε$^{-/-}$ B cells (solid line) against WT B cells (dotted line), for total naïve splenic B-cells stimulated with CpG. Error bars cover biological replicates (n = 3), and the * marks time points at which differences are statistically significant at $P < 0.05$, using a *t* test. (*H*) Representative mode-normalized fluorescence plots from dye dilution assays comparing proliferative capacities of IκBε$^{-/-}$ and WT B cells, for pure follicular naïve B-cells stimulated with LPS. (*I* and *J*) Line graphs of (*I*) population size over time (normalized to 48 h) and (*J*) growth rate (fold change per day), comparing IκBε$^{-/-}$ B cells (solid line) against WT B cells (dotted line), for pure follicular naïve B-cells stimulated with LPS. Error bars cover biological replicates (n = 4), and the * marks time points at which differences are statistically significant with $P < 0.05$, using a *t* test.

while both wild-type and IκBε$^{-/-}$ distributions have similar variance (CV ~ 0.36), there is an enrichment of high-expressing B cells in IκBε$^{-/-}$ relative to wild type, with about 8% of B cells shifting from the lower to the upper half of the cRel expression range. This supports the notion that IκBε negative feedback limits the excesses of cRel expression driven by intrinsic positive autoregulatory feedback.

Next, we asked whether IκBε controls the stimulus-responsive dynamics of cRel abundance. We cultured equal numbers of cRel$^{mTFP1/mTFP1}$ and cRel$^{mTFP1/mTFP1}$IκBε$^{-/-}$ B cells under identical CpG stimulation conditions in a 72-h time-course, as a parallel to our earlier comparison between cRel^{low} and cRel^{high} B cells (Fig. 3). Using the 15-h time point as the baseline, we compared dynamic changes in cRel abundance. Superposition of fluorescence distributions at various time points showed that IκBε$^{-/-}$ B cells initially had higher cRel, but were overtaken by wild-type B cells within 48 h (*SI Appendix*, Fig. S3*C*). Indeed, the rate of increase of cRel abundance was lower in IκBε$^{-/-}$ B cells compared to the wild type (*SI Appendix*, Fig. S3*D*). Thus, IκBε$^{-/-}$ B cells are composed of a greater number of high cRel expressors than the wild type, and their cRel expression dynamics also mimic those of cRel^{high} B cells relative to cRel^{low} B cells. These results support the notion that IκBε negative feedback strength is a mechanism determining cRel abundance and activation dynamics.

To examine how loss of damping of cRel expression by IκBε may affect the kinetics of B cell proliferative expansion, we compared the number of cell divisions across time points using dye dilution assays. While proliferation capacities at 72 h were similar, the expansion occurred earlier in IκBε$^{-/-}$ B cells than in the wild type (Fig. 4*E*). Specifically, we noted that population expansion mainly took place between 24 and 48 h in IκBε$^{-/-}$ B cells, but between 36 and 60 h in wild-type B cells. A closer inspection revealed that this is because most IκBε$^{-/-}$ B cells underwent their first division between 24 and 36 h, while most wild-type B cells began to divide between 36 and 48 h. These parallels of IκBε$^{-/-}$ to cRel^{high} B cells suggest that increased cRel abundance leads to reduced first division time, and therefore faster proliferative expansion.

We also plotted the fold change in population size over time for IκBε$^{-/-}$ and wild-type B cells (Fig. 4*F*), as well as their growth rates (Fig. 4*G*), for CpG stimulation. We found that IκBε$^{-/-}$ B cells reached their peak population size earlier than the wild type. However, this peak was smaller, and they were overtaken in numbers by wild-type B cells between 48 and 72 h. To confirm that these observations are independent of B cell subtype and stimulus, we repeated the dye dilution assays with pure follicular B cells stimulated with LPS and observed a similar pattern of an earlier but less sustained proliferative period in IκBε$^{-/-}$ follicular B cells (Fig. 4 *H*–*J*).

In summary, IκBε$^{-/-}$ B cells recapitulated the phenotype of cRel^{high} B cells in their increased steady-state cRel abundance, dynamical changes in cRel abundance on stimulation, and earlier but diminished proliferative expansion. From this correspondence

between IκBε$^{-/-}$ and cRel^{high} B-cells, we inferred that increased cRel abundance in B cells may arise due to diminished negative feedback by IκBε. This indicates that noisy IκBε feedback directs heterogeneous B cell proliferative responses by appropriate regulation of cRel dynamics.

Reduced IκBε Damping Increases cRel Activity but Not cMyc Induction. We next asked how variations in cRel abundance may give rise to its unexpected nonlinear relationship with proliferative outcomes in B cells. The nuclear activity of cRel is known to induce the expression of its target gene cellular Myelocytomatosis (cMyc) in response to stimulation, which in turn drives B cell growth and proliferation (8, 31, 32) (Fig. 5*A*). Prior studies based on flow cytometry using a cMyc-GFP reporter have shown that the amplitude of cMyc induction prior to the first division is proportional to the proliferative capacity of B cells (31, 32). However, flow cytometry is unable to resolve the active nuclear fractions of transcription factors from their whole cell abundances.

We looked at the dynamics of cRel nuclear activity and cMyc induction by immunoblotting nuclear lysates from wild-type and IκBε$^{-/-}$ splenic naïve B cells stimulated in vitro *SI Appendix*, Fig. S5*A*. We observed that cMyc induction closely tracked cRel activity, peaking around 4 to 6 h in both wild-type and IκBε$^{-/-}$ B cells, with similar temporal patterns upon stimulation with both CpG and LPS. IκBε$^{-/-}$ B cells, with diminished damping, showed increased basal activity of cRel, along with some basal cMyc induction. However, while the peak activity of cRel was also higher in IκBε$^{-/-}$, the corresponding induction of cMyc was not as high. We quantified the ratio of cMyc expression relative to cRel activity at the peak time point and found that IκBε$^{-/-}$ B cells produced proportionately less cMyc compared to the wild type. This suggests additional mechanisms that may limit cMyc induction by nuclear cRel.

To develop a quantitative understanding of this relationship between cRel activity and cMyc induction at single-cell resolution, we measured cRel and cMyc nuclear activities by microscopy using mTFP1-cRel and cMyc-GFP dual-reporter B cells, with and without IκBε, with the nucleus being resolved by the H2B-mCherry marker (Fig. 5*B* and *SI Appendix* SV4 and SV5). We compared snapshot distributions of nuclear fluorescence intensity at various times, using scatter plots to explore the relationship between cRel and cMyc (Fig. 5*C*), and connecting the distribution medians on violin plots to trace their population-averaged dynamics over time (Fig. 5 *D* and *E*). We found that IκBε$^{-/-}$ B cells, which have reduced damping, have a higher variability in basal nuclear activity of cRel, resulting in more outliers with slightly elevated basal cMyc expression. However, while the peak activity of cRel is higher in IκBε$^{-/-}$ B cells, the peak amplitude of induced cMyc is diminished. Interestingly, while visual inspection indicates that basal cMyc expression tracks basal cRel activity in IκBε$^{-/-}$ B cells, this relationship is not evident in the wild type. This indicates that basal cRel does not determine cMyc induction dynamics upon stimulation, and IκBε is necessary to enforce this relationship.

Overall, we conclude that B cells with less damping and higher cRel abundance (which are more abundant in the IκBε$^{-/-}$) are primed for earlier division, as a result of increases in basal cMyc which permits them to reach the threshold for activating the cell cycle earlier after stimulation. However, their subsequent reduction in peak cMyc amplitude cannot sustain their proliferative program for as long. This gives rise to the nonlinear relationship we observed between cRel abundance and B cell proliferative phenotype.

cMyc Amplitude Is Limited by Both Negative Feedback and Incoherent Feedforward Regulation. The population-level snapshots of cRel activity show a high degree of variability, particularly in IκBε$^{-/-}$ B cells, which is less pronounced in the case of cMyc expression. To better understand the nonlinear relationship between cRel activity and cMyc induction, we undertook live cell microscopy and tracked single B cells to measure trajectories of nuclear cRel activity and cMyc induction over 16 h (Fig. 6*A*). These trajectories are coupled within each B cell, allowing us to reveal correlations at single-cell resolution. We smoothed measured trajectory timepoints using a Savitzky–Golay filter, and quantified the basal and peak nuclear activities (Fig. 6*B*). Statistical analyses of the single-cell data (Fig. 6*C*) confirmed that IκBε$^{-/-}$ B cells showed a greater spread in basal levels of both cRel activity and cMyc expression, with more high-expressing outliers. However, their increased peak cRel activity produces less cMyc, consistent with our observations from population-level snapshot data (Fig. 5 *C*–*E*).

To dissect why more cRel activity does not directly lead to more cMyc induction, we plotted linear correlations between various dynamical features (defined in the *SI Appendix*, *Materials and Methods* section) for cRel activity and cMyc expression. We found that basal cRel activity is indeed strongly correlated to the basal expression of cMyc in IκBε$^{-/-}$ B cells. However, this relationship does not hold in wild-type B cells, in which basal cRel activity is tightly clustered at a lower range, and basal cMyc expression remains below a lower threshold than in IκBε$^{-/-}$ B cells (Fig. 6*D*). Thus, we concluded that cMyc induction is constrained by IκBε negative feedback at lower levels of cRel activity, where a portion of the measured nuclear cRel may be bound by IκBε and cannot induce transcription. When damping by IκBε is diminished, cMyc is elevated prior to stimulation. This may prime B cells for earlier cell cycle activation, leading to shorter first division times and increased early proliferation.

We next looked at what features of cRel activity may determine the peak amplitude of cMyc, which was reported to determine B cell proliferative capacity (31, 32). We found that in both wild-type and IκBε$^{-/-}$ B cells, variability in peak cMyc amplitudes is poorly explained by the corresponding peak cRel activities (Fig. 6*E*). Specifically, we observed that increases in peak cRel activity do not produce a corresponding rise in cMyc expression (Fig. 6*E*). However, peak cMyc expression is better correlated with the activation rate of cRel in both wild-type and IκBε$^{-/-}$ B cells (Fig. 6*F*). This suggests that an incoherent feedforward mechanism limits the expression of cMyc at higher levels of cRel activity, which may be mediated by an additional target gene of cRel that inhibits the production of cMyc. Prior studies have indicated that other NFκB dimers containing p50 and/or RelB, which are target genes of cRel or RelA, may provide such inhibition, by competing with cRel to bind the κB motif on DNA but failing to activate transcription at these loci (33, 34).

Incoherent feedforward loops may further act as fold change detectors under the condition where the expression of the output gene is strongly inhibited (33, 35, 36). We found that among all the features of cRel dynamics in wild-type B cells, the fold change in cRel activity was best correlated to peak cMyc amplitude, explaining about half its variation (Fig. 6*G*). Together with the lack of correlation with either basal or peak cRel activity (Fig. 6 *E* and *F*), this indicates that the incoherent feed-forward loop regulating the peak amplitude of cMyc may indeed decode the fold change in cRel activity. Surprisingly, we found that this fold change detection property is entirely lost in IκBε$^{-/-}$ B cells (Fig. 6*G*). From this, we inferred that negative feedback by IκBε is necessary for sufficiently strong inhibition of cMyc, particularly at lower levels of cRel activity. Taken together, we suggest that negative feedback and incoherent feedforward loops synergize to inhibit cMyc production across the dynamic range of cRel nuclear activities, revealing intricate control of cMyc induction following B cell stimulation.

We then modified the mathematical model of cRel-dependent B cell proliferation to include the incoherent feedforward regulation

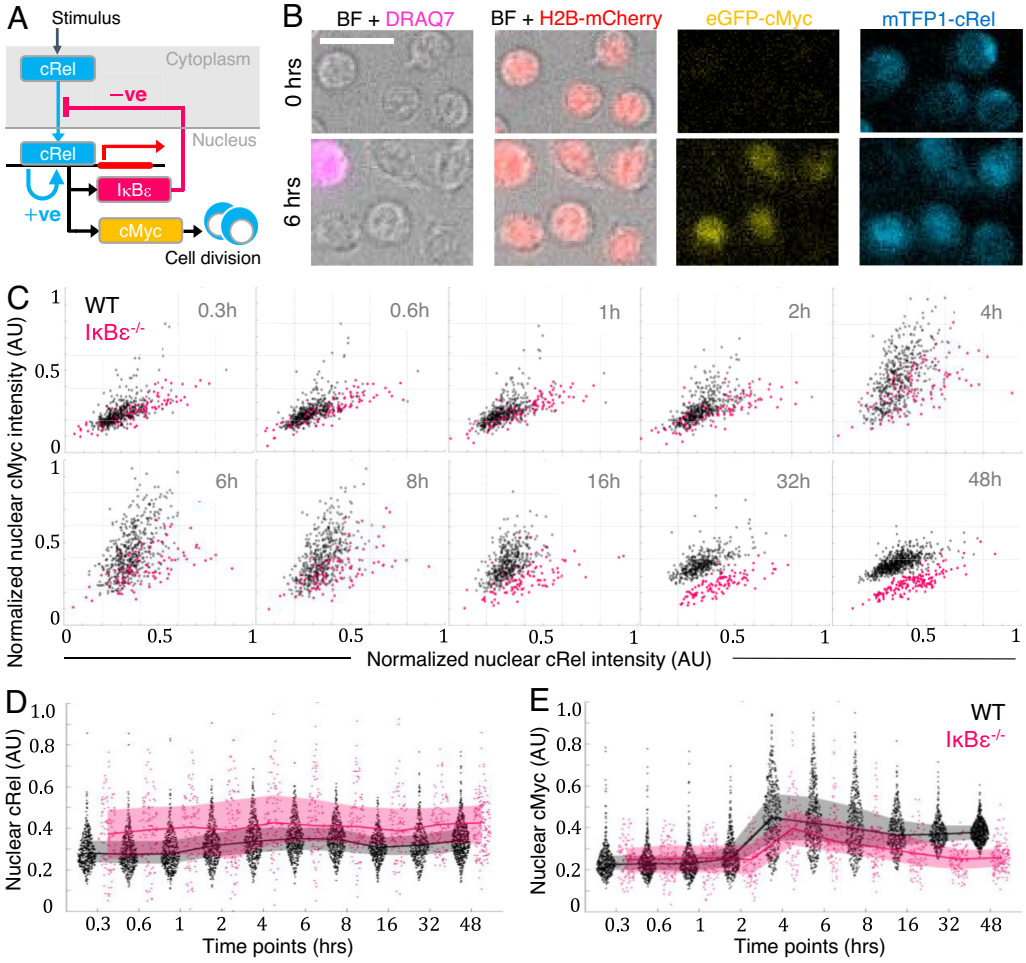

Fig. 5. Diminished damping of cRel by IκBε increases its basal nuclear activity to prime cells for early proliferation but reduces induction of cMyc. (*A*). Schematic of negative feedback regulation of cRel dynamics and B cell proliferation, showing stimulus-induced cRel nuclear translocation, followed by induction of the pro-proliferative target gene cMyc, in addition to cRel itself, as well as IκBε leading to damping of nuclear cRel activity. (*B*) Multichannel fluorescence microscopy images of live mTFP1-cRel cMyc-GFP dual-reporter B-cells at 40×/NA1.3 under oil immersion. Panels in order show brightfield images with DRAQ7 viability staining (deep red), H2B-mCherry (red) as a marker distinguishing the nuclear compartment, with cMyc-GFP expression (yellow) and mTFP1-cRel (blue) nuclear localization compared at the 0 h baseline and 6 h poststimulation with CpG. (*C*) Scatter plots of nuclear cRel activity and cMyc expression in individual B cells, comparing WT (n = ~700) and IκBε$^{-/-}$ (n = ~160) B cells across 48 h after CpG stimulation. (*D and E*) Violin plots from the above scatter plots showing the distribution of (*D*) nuclear cRel activity and (*E*) induced cMyc expression over time, in single WT and IκBε$^{-/-}$ B cells following CpG stimulation. The solid lines connect median values of the respective distributions at each time point, with the interquartile range marked by the shaded region.

of cMyc by cRel, along with IκBε negative feedback (Fig. 6*H*). While the increase in basal cMyc expression was preserved in both the original and modified models, the addition of the incoherent feedforward loop was essential for computationally reproducing the reduction in peak cMyc amplitude in IκBε$^{-/-}$ B cells, which was not possible through direct regulation alone (Fig. 6*I*). This is a unique prediction of the model, validated by our experimental data. We then analyzed its impact on proliferative kinetics, by computationally simulating stimulus-driven proliferation over 72 h for equal starting populations of wild-type and IκBε$^{-/-}$ founder B cells, with and without the feedforward inhibition of cMyc. Histograms of the terminal generation (total number of divisions) reached by founder B cells showed that incoherent feedforward regulation is necessary to recapitulate the termination of IκBε$^{-/-}$ B cell proliferation after fewer divisions (Fig. 6*J*). Under feedforward inhibition, fewer IκBε$^{-/-}$ founder B cells than the wild type sustained their proliferation to reach five or more divisions, being preferentially limited to four or fewer divisions. This trend was reversed in the absence of such feedforward inhibition. This comparison across generations is summarized by the lower ratio of IκBε$^{-/-}$ to wild-type founder B cells reaching later generations under incoherent feedforward regulation, indicating that this mechanism constrains B cell proliferation even in the absence of damping by IκBε (Fig. 6*J*).

Finally, we compared our computational results to experimental dye dilution data with the same stimulus and dose from Fig. 4 *E–G*. For experimental data, we estimated the division index (average number of divisions for cells entering the proliferative program) using a FlowJo proliferation analysis. For simulated cells, we calculated the mean division number, to compare the equivalent kinetic trends in proliferation over time. Simulations with incoherent feedforward regulation of cMyc recapitulated the diminished rate of late proliferation in IκBε B cells. This allowed wild-type B cells to catch up despite delayed activation of the proliferative program, matching experimentally observed trends (Fig. 6*K*).

In sum, analysis of temporal trajectories enabled by live cell imaging of triple reporter B cells suggests that cMyc peak abundance, which determines proliferative capacity in the clonal burst, is determined by fold change of cRel activation interpreted by an incoherent feedforward loop, and that IκBε negative feedback is critical to safeguard this relationship.

Discussion

In this work, we examined whether and how NFκB cRel is a determinant of the stimulus-responsive proliferative burst of B-cells. Prior work established the necessity of cRel in B cell proliferation (7), but did not reveal the quantitative relationship between cRel abundances and the resulting proliferation dynamics. Here, we presented a live cell fluorescent reporter of cRel expression, measured the natural variation in cRel abundance within naïve unstimulated B cells, and related it to proliferative outcomes upon stimulation. We found that the relationship between cRel abundance and B cell proliferation is unexpectedly complex. Naïve B cells with high cRel abundance activated the proliferative program faster, but unexpectedly they produced fewer progeny overall as they did not sustain the proliferative program. Using model-directed experimental studies, we identified the negative feedback regulator IκBε as a key regulator of variable cRel expression, and cMyc as a mediator of phenotypic heterogeneity.

To measure and quantify cRel abundances within live intact primary B cells that are capable of further proliferation, we generated

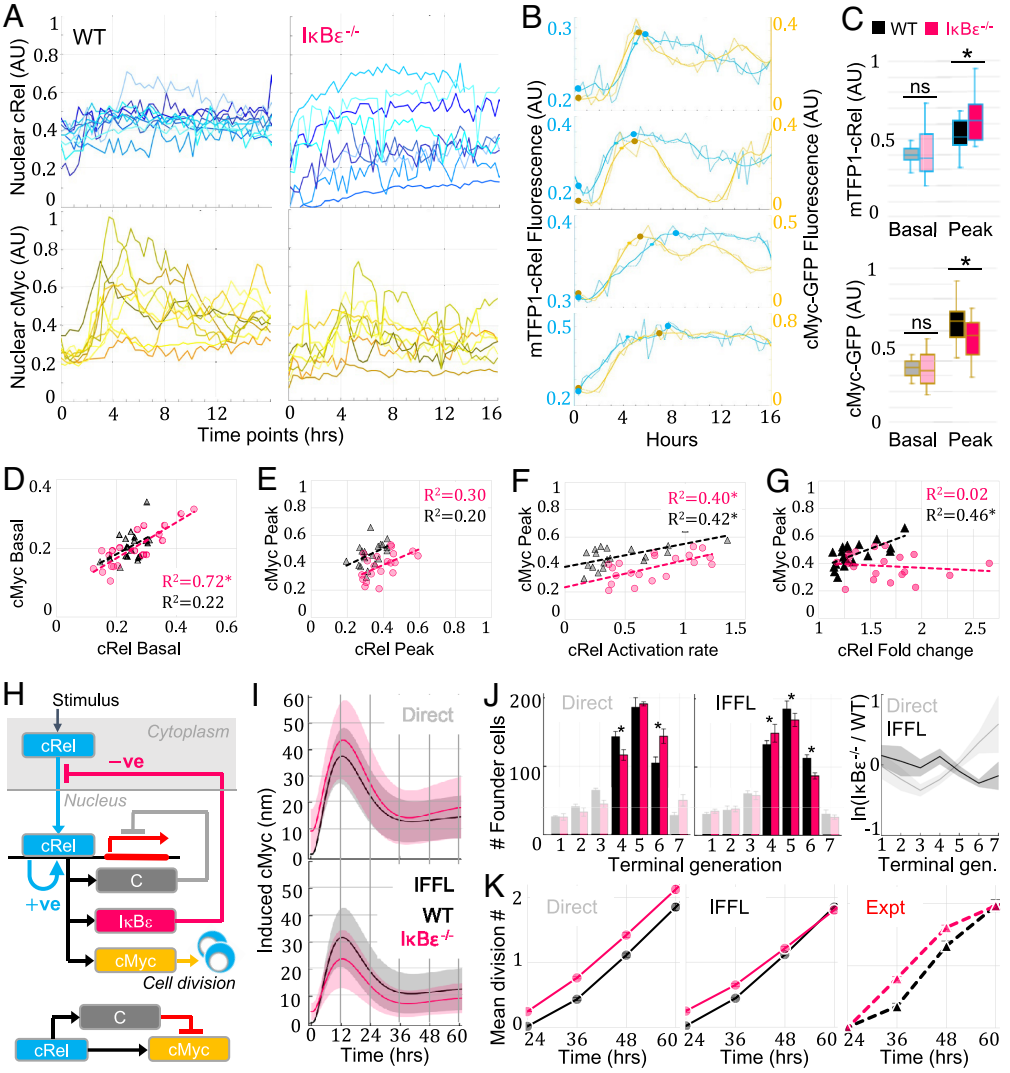

Fig. 6. Incoherent feedforward regulation limits the amplitude of cMyc induction. (*A*) Representative trajectories for cRel nuclear activity and cMyc induction in WT and IκBε$^{-/-}$ B cells. (*B*) Coupled trajectories of cRel nuclear activity (blue) and cMyc induction (yellow) dynamics within representative B cells. The basal and peak amplitudes are marked with filled circles. (*C*) Distributions of peak and basal cRel nuclear activity and cMyc induction across single B cells (n = 20 cells each for WT and IκBε$^{-/-}$). The * indicates significant differences using a paired *t* test, at $P < 0.01$ for the given sample size. (*D–G*) Correlations between dynamical features of cRel activity and cMyc expression among WT (black triangles) and IκBε$^{-/-}$ (pink circles) B cells (n = 20 cells each for WT and IκBε$^{-/-}$). Regression lines for each genotype are drawn separately, with Pearson coefficients of determination R^2 indicated on the plot. An * beside the R^2 value indicates significance of the correlation at $P < 0.01$ for the given sample size. (*H*) Schematic of regulation of B cell proliferation by cRel dynamics, showing induction of its target genes cRel, IκBε, cMyc, and a competitor C that may inhibit transactivation by cRel. The competitor-mediated incoherent feedforward loop regulating cMyc in response to cRel is shown in gray, and the IκBε negative feedback loop damping cRel is in pink. (*I*) Simulated cMyc induction in WT and IκBε$^{-/-}$ B cells, in response to canonical IKK inputs measured using western blots following 250 nM CpG stimulation, in the absence (*Top*) and presence (*Bottom*) of feedforward inhibition of cRel-mediated transcription by a competitor. (*J*) Simulated histograms comparing the number of founder B cells from WT (black bars) and IκBε$^{-/-}$ (pink bars) that have reached different terminal generations at 72 h poststimulation, in the absence (*Left*) and presence (*Middle*) of feedforward inhibition of cRel-mediated transcription by a competitor. Generations 4 to 6 are emphasized to highlight the range where meaningful differences alter the population composition. Error bars indicate variations across 5 simulation runs starting with 1,000 founder cells each. An * above a pair of bars indicates a statistically significant difference at $P \leq 0.05$ between the number of WT and IκBε$^{-/-}$ founder B cells reaching that generation. The logarithmic ratio of WT and IκBε$^{-/-}$ founder B cell numbers reaching each terminal generation is plotted on the *Right*. (*K*) Comparison of kinetic trends in proliferation between simulation and experiments for wild-type (black) and IκBε$^{-/-}$ (pink) founder B cells. The mean division number was calculated for simulated data (solid lines with circles) in the absence (*Left*) and presence (*Middle*) of feedforward inhibition of cRel-mediated transcription by a competitor. Error bars indicate variations across 5 simulation runs starting with 1,000 founder cells each. The equivalent division index was derived with the FlowJo proliferation analysis module (*Right*, dotted lines with triangles), using dye dilution experimental data from Fig. 5 *E–G* corresponding to the simulated condition (stimulation with 250 nM CpG). Error bars were calculated across three biological replicates.

a mouse strain with the fluorescent gene mTFP1 knocked into exon 2 of the endogenous cRel locus. This design choice avoids affecting promoter-driven expression control of cRel that may occur when altering exon 1. We showed that the fusion protein undergoes no unwanted proteolysis, and faithfully captures the cellular abundance and nuclear activity of cRel in naïve splenic B cells (Fig. 1). There are some proliferative defects in homozygous reporter B cells, potentially due to impaired gene activation functions, but heterozygous reporter B cells are unaffected. This characterization of functional outcomes may help in choosing the appropriate combination of alleles for future studies using this reporter, with homozygosity suitable for accurately measuring cRel abundance, and heterozygosity preferable for measuring proliferation.

Our choice of mTFP1-cRel in the blue wavelength spectrum distinguishes this mouse strain from a recently reported mScarlet-cRel mouse strain (16). We showed that this reporter is compatible for live cell imaging studies with other reporters, such as mVenus-RelA (19) or cMyc-EGFP (37), and leaves longer wavelengths open for multiplexing with other reporters for multidimensional trajectory measurements. We leveraged this to develop a microscopy workflow with H2B-mCherry for imaging nuclear activity of transcription factors in B cells, overcoming the challenges of small size of the cells, thin cytoplasm, and lack of adherence at the initial stage followed by high motility upon activation. While the movement of transcription factors between nuclear and cytoplasmic compartments has been measured in various cell types with larger size, such as macrophages (19) or HeLa cells (33), only one other study to our knowledge has imaged their nuclear activity in primary lymphocytes (38).

We quantified the steady-state cellular abundance of cRel and found it to be heterogeneous yet reproducible across individuals, and stably maintained over time in the absence of stimulation (Fig. 2). Heavy-tailed distributions have previously been described for protein abundances within cells (39). Among these, lognormal distributions may be expected to arise as the result of random variations accumulating across mutually independent regulatory processes (22, 40). However, this is a rough approximation with deviations in the limit

of bursty transcription, and may also arise from other underlying mechanisms (22). Empirical studies have suggested that cellular species abundances are better described by the PLN distribution, which is log-normal around the median but with fat tails approximating power laws (24, 41). This distribution is hypothesized to arise when regulatory processes are not mutually independent, but fully or partially connected by both positive and negative feedback loops, producing more outliers than expected by chance alone (24). In addition, the stability of cRel whole cell and nuclear concentrations further indicates that regulatory feedback loops may contribute to persistence in protein levels (20). Thus, the cRel distribution was consistent with a PLN distribution, and the enrichment for high-expressing cells cannot be explained by cell size alone. Taken together, these observations suggest that cRel abundance in naïve B cell populations in vivo is tightly regulated by cell-intrinsic feedback mechanisms.

Heterogeneity in signaling proteins has been shown earlier to modulate phenotypic differences across a population of immune cells, such as antigen responsiveness in T-cells. Here, we asked whether the fat-tailed heterogenous distribution of cRel in B cells modulates stimulus-responsive proliferation. We found that B cells with high basal cRel levels were capable of activating the proliferative program faster, but paradoxically they showed a reduced total population size, since they underwent fewer divisions on average (Fig. 3). Thus, cRel abundance correlates with both activating and terminating B cell proliferation. Such complexities in the relationship cannot be anticipated from gene knockout studies, but are revealed by leveraging natural variation for direct observational studies.

Stimulation of B cells activates both cRel and RelA, which typically bind to the same kB motifs in most target gene promoters (42, 43). We leveraged the dual reporter to show that cRel and RelA abundances are highly correlated in B cells. However, we also showed that RelA cannot rescue stimulus-dependent B cell proliferation in the absence of cRel, indicating that B cell proliferative outcomes are primarily determined by cRel (*SI Appendix*, Fig. S2). This could be a consequence of dynamical variations in activity, since RelA has a more transient activity in the nucleus upon stimulation compared to cRel (*SI Appendix*, Fig. S1*D*).

Our findings may also provide mechanistic insight for previously reported differences between subpopulations of splenic B cells. While marginal zone (MZ) B cells (typically forming 5 to 9% of wild-type naïve splenic B cells) are known to proliferate faster but with reduced proliferative capacity in response to LPS, compared to follicular (FO) B cells (29, 30), the molecular mechanism for this distinction was unclear. Our study suggests that high cRel expression may have a causal role, and that newly maturing naïve B cells escaping IκBε buffering to produce the heavy tailed distribution of high cRel expression may generate a MZ B cell population (*SI Appendix*, Fig. S4). This is supported by the observation that IκBε$^{-/-}$ mice have greater proportions of MZ B cells (up to 20% of splenic B cells) (30).

The negative feedback regulator IκBε was previously shown to have the potential to increase the heterogeneity of stimulus-driven NFκB oscillations (44, 45). Indeed, by knocking out IκBε in our reporter mouse strain, we found that the IκBε$^{-/-}$ B cells had a larger proportion expressing high levels of cRel compared to the wild type. Thus, IκBε negative feedback constrains the spread of the distribution, by limiting excess cRel expression in the population. However, IκBε expression is notably noisy due to epigenetic stochasticity in its induction (46), allowing cRel expression to escape the IκBε buffering mechanism in some cells. As a result, we see an enrichment of B cells with more cRel abundance, including the extreme outliers forming the heavy tails of the cRel distribution in wild-type B cell populations (Fig. 4).

The complex cell population dynamics were also reflected in the dynamics of cRel abundance. cRel is known to positively regulate itself through autoinduction (26). B cells with higher basal cRel levels attain lower levels of induced cRel, although in a shorter period of time (Figs. 3 and 4). This damping of cRel at later times may involve negative feedback mechanisms other than IκBε, via signaling regulatory mechanisms such as A20 or the IκBsome, or via mechanisms that control metabolic capacity.

cRel is also known to induce the target gene cMyc to trigger growth and cell cycle entry (8), where the amplitude of cMyc determines the proliferative capacity (32). We leveraged our microscopy workflow to resolve nuclear cRel and study its relationship to cMyc induction (Figs. 5 and 6). We found that damping by IκBε keeps basal cMyc levels tightly in check at low levels of cRel activity, preventing cell cycle activation in the absence of stimulation. However, elevated basal cRel in the absence of damping by IκBε produces higher basal cMyc expression, priming these B cells for division, potentially by crossing the threshold for cell cycle entry earlier. Yet, in this context, higher peak activity of cRel does not translate into higher amplitudes of cMyc expression, suggesting that incoherent feedforward regulation limits cMyc expression as cRel activity increases. This effect is stronger in wild-type B cells, where cMyc responds to the fold change of nuclear cRel, but weaker in IκBε$^{-/-}$ B cells where the fold change detection property disappears. Fold change detection has previously been described for target genes of NFκB RelA, where the p50:p50 homodimer was hypothesized as the inhibitor of RelA target gene expression, by competing for binding to κB sites in gene promoters without driving any transcriptional activation (33, 34). Our prior work has shown a hyperproliferative phenotype in *nfkb1*$^{-/-}$ B cells which lack p50, consistent with this mechanism (47). It is possible that there may also be other species involved in the competitive inhibition of cRel binding, such as dimers containing RelB (48).

Our results show that IκBε feedback regulation of cRel activity and incoherent feedforward regulation of cMyc expression act synergistically to regulate proliferative outcomes. However, the dynamics of cRel activity explain only about half the variations in cMyc expression, suggesting that cMyc may also be controlled by other pathways independent of cRel, such as the MAPK pathway. Further, there may also be regulatory architectures other than the incoherent feedforward loop that constrain cMyc expression. cMyc itself has been shown to activate E2F through incoherent feedforward regulation (49), as an additional restraint prior to cell cycle activation. Together, this highlights the multiple layers of complex regulatory control between cRel, cMyc, and cell cycle progression, which may safeguard against the uncontrolled proliferation of B cells in response to ectopic stimuli.

The dual relationship of cRel in activating vs. sustaining the proliferative program reconciles conflicting reports in the literature—whereas experimental knockout studies established that cRel is required to activate proliferation in a dose-dependent manner (7), computational modeling studies suggested that regulators other than cRel determine the proliferative capacity (5). This emphasizes that the identification of a genetic requirement does not necessarily imply regulatory control of the phenotypic outcomes in the natural context. Therefore, complementing gene knockout approaches with direct observational studies is critical, and can reveal unforeseen complexities in the quantitative regulatory relationships determining the behavior of biological systems.

The changes and effect sizes observed here are relatively subtle in many cases, with proliferative differences being around twofold to threefold between cells with more or less cRel. However, these are consistently observed across multiple stimuli, B cell subtypes, and experimental modalities. Further, rigorous statistical testing consistently upheld these differences, with small P-values ($P < 0.01$ in many cases) providing confidence that the observations represent the underlying biology and not merely random fluctuations in small sample sizes. The results presented here represent the outcomes of a single round of a proliferative burst in vitro. However, follicular

B cells typically undergo multiple (around 20 to 30) rounds of proliferative expansion in successive clonal bursts in vivo during the germinal center response (2). Thus, even subtle differences in proliferative responses may compound exponentially over this period, to exert a substantial effect on antibody response outcomes.

In summary, the timing and extent of B cell proliferative expansion in response to a given stimulus is highly variable. This heterogeneity is an intrinsic feature of the intricate regulatory control of cRel abundance and B cell proliferation. This raises the question of why such heterogeneity and feedback regulation is required in the B cell response, and what its functional consequences may be. Phenotypic heterogeneity has been proposed to facilitate "bet-hedging" among populations, to adapt to fluctuating conditions (50). Other contexts within the immune response have established that precocious responders can influence the response, and enable complex dynamical trajectories by balancing positive and negative feedback mechanisms (51). Here, we report that B cell populations are enriched for outliers with high cRel expression, which could accelerate an early response, while the later response favors B-cells that show a high fold-induction in cRel upon stimulation. Our results reflect that it may be beneficial that early dividers do not go on to dominate the population, but leave room for higher-affinity B cells that experience high stimulus-responsive activation.

Data, Materials, and Software Availability. All raw data corresponding to flow cytometry and proliferation time courses are available as FCS files. Raw data from live cell imaging are available as CZI files. These are available for download on Dryad at https://doi.org/10.5061/dryad.cfxpnvxdk. Python coding notebooks with statistical analyses of flow data, Julia coding notebooks for the mathematical modeling, and MATLAB or Fiji scripts for image analysis are all available on the Signaling Systems Lab GitHub at https://github.com/signalingsystemslab/mTFP1-cRel_DirectObservationBcells.

ACKNOWLEDGMENTS. We thank the current and former members of the Hoffmann and Roy labs for valuable discussions and feedback on the manuscript. We also thank Roy Wollman, Zach Hemminger, Pavak Shah, and the Kueh lab at the University of Washington, Seattle for valuable inputs in designing the microscopy and image analysis pipelines. A.H. acknowledges funding from sources R01AI132731 and R01AI127867. K.R. acknowledges funding from the American Society of Hematology Scholar Award R56AI177789, and the Department of Pathology, University of Utah. H.V.N. acknowledges support from the James S. McDonnell Foundation Postdoctoral Fellowship and the Damon Runyon Quantitative Biology Fellowship.

Author affiliations: [a]Signaling Systems Laboratory, Department of Microbiology, Immunology, and Molecular Genetics, University of California Los Angeles, Los Angeles, CA 90095; [b]Institute for Quantitative and Computational Biosciences, University of California Los Angeles, Los Angeles, CA 90095; and [c]Division of Microbiology and Immunology, Department of Pathology, University of Utah, Salt Lake City, UT 84112

1. F. M. Burnet, A modification of Jerne's theory of antibody production using the concept of clonal selection. *Aust. J. Sci.* **20**, 67–69 (1957).
2. G. D. Victora, M. C. Nussenzweig, Germinal centers. *Annu. Rev. Immunol.* **40**, 413–442 (2022).
3. A. B. Lyons, C. R. Parish, Determination of lymphocyte division by flow cytometry. *J. Immunol. Methods* **171**, 131–137 (1994).
4. E. D. Hawkins, J. F. Markham, L. P. McGuinness, P. D. Hodgkin, A single-cell pedigree analysis of alternative stochastic lymphocyte fates. *Proc. Natl. Acad. Sci. U.S.A.* **106**, 13457–13462 (2009).
5. S. Mitchell, K. Roy, T. A. Zangle, A. Hoffmann, Nongenetic origins of cell-to-cell variability in B lymphocyte proliferation. *Proc. Natl. Acad. Sci. U.S.A.* **115**, E2888–E2897 (2018).
6. R. J. Grumont *et al.*, B lymphocytes differentially use the Rel and nuclear factor kappaB1 (NF-kappaB1) transcription factors to regulate cell cycle progression and apoptosis in quiescent and mitogen-activated cells. *J. Exp. Med.* **187**, 663–674 (1998).
7. F. Köntgen *et al.*, Mice lacking the c-rel proto-oncogene exhibit defects in lymphocyte proliferation, humoral immunity, and interleukin-2 expression. *Genes Dev.* **9**, 1965–1977 (1995).
8. R. J. Grumont, A. Strasser, S. Gerondakis, B cell growth is controlled by phosphatidylinosotol 3-kinase-dependent induction of Rel/NF-kappaB regulated c-myc transcription. *Mol. Cell* **10**, 1283–1294 (2002).
9. M. N. Shokhirev *et al.*, A multi-scale approach reveals that NF-κB cRel enforces a B-cell decision to divide. *Mol. Syst. Biol.* **11**, 783 (2015).
10. J. Larsch, D. Ventimiglia, C. I. Bargmann, D. R. Albrecht, High-throughput imaging of neuronal activity in Caenorhabditis elegans. *Proc. Natl. Acad. Sci. U.S.A.* **110**, E4266–E4273 (2013).
11. S. Chen, A. Y. Lee, N. M. Bowens, R. Huber, E. A. Kravitz, Fighting fruit flies: A model system for the study of aggression. *Proc. Natl. Acad. Sci. U.S.A.* **99**, 5664–5668 (2002).
12. L. A. Sawyer *et al.*, Natural variation in a Drosophila clock gene and temperature compensation. *Science* **278**, 2117–2120 (1997).
13. G. Wang *et al.*, First quantitative high-throughput screen in zebrafish identifies novel pathways for increasing pancreatic β-cell mass. *Elife* **4**, e08261 (2015).
14. M. J. T. Stubbington, O. Rozenblatt-Rosen, A. Regev, S. A. Teichmann, Single-cell transcriptomics to explore the immune system in health and disease. *Science* **358**, 58–63 (2017).
15. J. D. Buenrostro *et al.*, Single-cell chromatin accessibility reveals principles of regulatory variation. *Nature* **523**, 486–490 (2015).
16. S. M. T. Rahman *et al.*, Double knockin mice show NF-κB trajectories in immune signaling and aging. *Cell Rep.* **41**, 111682 (2022).
17. N. Heise *et al.*, Germinal center B cell maintenance and differentiation are controlled by distinct NF-κB transcription factor subunits. *J. Exp. Med.* **211**, 2103–2118 (2014).
18. K. Roy *et al.*, A regulatory circuit controlling the dynamics of NFκB cRel transitions B cells from proliferation to plasma cell differentiation. *Immunity* **50**, 616–628.e6 (2019).
19. A. Adelaja *et al.*, Six distinct NFκB signaling codons convey discrete information to distinguish stimuli and enable appropriate macrophage responses. *Immunity* **54**, 916–930.e7 (2021).
20. A. Sigal *et al.*, Variability and memory of protein levels in human cells. *Nature* **444**, 643–646 (2006).
21. O. Feinerman, J. Veiga, J. R. Dorfman, R. N. Germain, G. Altan-Bonnet, Variability and robustness in T cell activation from regulated heterogeneity in protein levels. *Science* **321**, 1081–1084 (2008).
22. A. L. Koch, The logarithm in biology 1. Mechanisms generating the log-normal distribution exactly. *J. Theor. Biol.* **12**, 276–290 (1966).
23. S. L. Spencer, S. Gaudet, J. G. Albeck, J. M. Burke, P. K. Sorger, Non-genetic origins of cell-to-cell variability in TRAIL-induced apoptosis. *Nature* **459**, 428–432 (2009).
24. C. Lu, R. D. King, An investigation into the population abundance distribution of mRNAs, proteins, and metabolites in biological systems. *Bioinformatics* **25**, 2020–2027 (2009).
25. B. Peng *et al.*, Defective feedback regulation of NF-κB underlies Sjögren's syndrome in mice with mutated κB enhancers of the IκBα promoter. *Proc. Natl. Acad. Sci. U.S.A.* **107**, 15193–15198 (2010).
26. M. Hannink, H. M. Temin, Structure and autoregulation of the c-rel promoter. *Oncogene* **5**, 1843–1850 (1990).
27. S. Mitchell, R. Tsui, Z. C. Tan, A. Pack, A. Hoffmann, The NF-κB multidimer system model: A knowledge base to explore diverse biological contexts. *Sci. Signal.* **16**, eabo2838 (2023).
28. A. Cerutti, M. Cols, I. Puga, Marginal zone B cells: Virtues of innate-like antibody-producing lymphocytes. *Nat. Rev. Immunol.* **13**, 118–132 (2013).
29. A. M. Oliver, F. Martin, G. L. Gartland, R. H. Carter, J. F. Kearney, Marginal zone B cells exhibit unique activation, proliferative and immunoglobulin secretory responses. *Eur. J. Immunol.* **27**, 2366–2374 (1997).
30. B. N. Alves *et al.*, IκBε is a key regulator of B-cell expansion by providing negative feedback on cRel and RelA in a stimulus-specific manner. *J. Immunol.* **192**, 3121–3132 (2014).
31. S. Finkin, H. Hartweger, T. Y. Oliveira, E. E. Kara, M. C. Nussenzweig, Protein amounts of the MYC transcription factor determine germinal center B cell division capacity. *Immunity* **51**, 324–336.e5 (2019).
32. S. Heinzel *et al.*, A Myc-dependent division timer complements a cell-death timer to regulate T cell and B cell responses. *Nat. Immunol.* **18**, 96–103 (2017).
33. R. E. C. Lee, S. R. Walker, K. Savery, D. A. Frank, S. Gaudet, Fold change of nuclear NF-κB determines TNF-induced transcription in single cells. *Mol. Cell* **53**, 867–879 (2014).
34. V. C. Wong, S. Mathew, R. Ramji, S. Gaudet, K. Miller-Jensen, Fold-change detection of NF-κB at target genes with different transcript outputs. *Biophys. J.* **116**, 709–724 (2019).
35. L. Goentoro, O. Shoval, M. Kirschner, U. Alon, The incoherent feedforward loop can provide fold-change detection in gene regulation. *Mol. Cell* **36**, 894–899 (2009).
36. M. Adler, U. Alon, Fold-change detection in biological systems. *Curr. Opin. Syst. Biol.* **8**, 81–89 (2018).
37. C.-Y. Huang, A. L. Bredemeyer, L. M. Walker, C. H. Bassing, B. P. Sleckman, Dynamic regulation of c-Myc proto-oncogene expression during lymphocyte development revealed by a GFP-c-Myc knock-in mouse. *Eur. J. Immunol.* **38**, 342–349 (2008).
38. M. J. Wither *et al.*, Antigen perception in T cells by long-term Erk and NFAT signaling dynamics. *Proc. Natl. Acad. Sci. U.S.A.* **120**, e2308366120 (2023).
39. Y. Taniguchi *et al.*, Quantifying E. coli proteome and transcriptome with single-molecule sensitivity in single cells. *Science* **329**, 533–538 (2010).
40. S. Krishna, B. Banerjee, T. V. Ramakrishnan, G. V. Shivashankar, Stochastic simulations of the origins and implications of long-tailed distributions in gene expression. *Proc. Natl. Acad. Sci. U.S.A.* **102**, 4771–4776 (2005).
41. W. J. Reed, The Pareto law of incomes–An explanation and an extension. *Phys. A: Stat. Mech. Appl.* **319**, 469–486 (2003).
42. M. Zhao *et al.*, NF-κB subunits direct kinetically distinct transcriptional cascades in antigen receptor-activated B cells. *Nat. Immunol.* **24**, 1552–1564 (2023).
43. K. Roy, M. Chakraborty, A. Kumar, A. K. Manna, N. S. Roy, The NFκB signaling system in the generation of B-cell subsets: From germinal center B cells to memory B cells and plasma cells. *Front. Immunol.* **14**, 1185597 (2023).
44. P. Paszek *et al.*, Population robustness arising from cellular heterogeneity. *Proc. Natl. Acad. Sci. U.S.A.* **107**, 11644–11649 (2010).
45. J. D. Kearns, S. Basak, S. L. Werner, C. S. Huang, A. Hoffmann, IκBε provides negative feedback to control NF-κB oscillations, signaling dynamics, and inflammatory gene expression. *J. Cell Biol.* **173**, 659–664 (2006).
46. L. Ashall *et al.*, Pulsatile stimulation determines timing and specificity of NF-kappa B-dependent transcription. *Science* **324**, 242–246 (2009).
47. M. N. Shokhirev, A. Hoffmann, FlowMax: A computational tool for maximum likelihood deconvolution of CFSE time courses. *PLoS One* **8**, e67620 (2013).
48. H. I. Navarro *et al.*, RelB-deficient autoinflammatory pathology presents as interferonopathy, but in mice is interferon-independent. *J. Allergy Clin. Immunol.* **152**, 1261–1272 (2023).
49. K. A. O'Donnell, E. A. Wentzel, K. I. Zeller, C. V. Dang, J. T. Mendell, c-Myc-regulated microRNAs modulate E2F1 expression. *Nature* **435**, 839–843 (2005).
50. M. Ackermann, A functional perspective on phenotypic heterogeneity in microorganisms. *Nat. Rev. Microbiol.* **13**, 497–508 (2015).
51. A. K. Shalek *et al.*, Single-cell RNA-seq reveals dynamic paracrine control of cellular variation. *Nature* **510**, 363–369 (2014).